We are IntechOpen,
the world's leading publisher of Open Access books
Built by scientists, for scientists

5,800
Open access books available

142,000
International authors and editors

180M
Downloads

154
Countries delivered to

Our authors are among the

TOP 1%
most cited scientists

12.2%
Contributors from top 500 universities

CLARIVATE ANALYTICS
BOOK CITATION INDEX
INDEXED

WEB OF SCIENCE™

Selection of our books indexed in the Book Citation Index
in Web of Science™ Core Collection (BKCI)

Interested in publishing with us?
Contact book.department@intechopen.com

Numbers displayed above are based on latest data collected.
For more information visit www.intechopen.com

Modeling the Bulk and Nanometric Dielectric Functions of Au and Ag

Brahim Ait Hammou, Abdelhamid El Kaaouachi,
Abdellatif El Oujdi, Adil Echchelh, Said Dlimi,
Chi-Te Liang and Jamal Hemine

Abstract

In this work, we model the dielectric functions of gold (Au) and silver (Ag) which are typically used in photonics and plasmonics. The modeling has been performed on Au and Ag in bulk and in nanometric states. The dielectric function is presented as a complex number with a real part and an imaginary part. First, we will model the experimental measurements of the dielectric constant as a function of the pulsation ω by appropriate mathematical functions in an explicit way. In the second part we will highlight the contributions to the dielectric constant value due to intraband and interband electronic transitions. In the last part of this work we model the dielectric constant of these metals in the nanometric state using several complex theoretical models such as the Drude Lorentz theory, the Drude two-point critical model, and the Drude three-point critical model. We shall comment on which model fits the experimental dielectric function best over a range of pulsation.

Keywords: Modeling bulk and nanometric dielectric function, noble metals Au and Ag, interband transitions, intraband transitions, UV and IR pulsations

1. Introduction

All the intrinsic effects corresponding to the process of light-matter interaction are contained in the dielectric function $\varepsilon(\omega)$. In the case of an isotropic material, the optical response is described by following equation

$$\varepsilon(\omega) = \varepsilon_1(\omega) + i\varepsilon_2(\omega) \tag{1}$$

where $\varepsilon(\omega)$ is generally a complex scalar value which depends upon the pulsation ω of the field. If the medium has an anisotropy, this magnitude is in the form of a tensor. It is often convenient to describe the optical response in an equivalent way from the complex refractive index $\tilde{n} = n + i\kappa$ as n denotes the refractive index describing the phase speed of the wave and κ denotes the extinction index describing the absorption of the wave during propagation in the material. These two indices are directly related to the dielectric constant of the material. In fact, the real and imaginary parts of the dielectric function are deduced from the relation:

$$\varepsilon_1 = n^2 - \kappa^2 \tag{2}$$

$$\varepsilon_2 = 2n\kappa \tag{3}$$

Several important physical quantities can be deduced from the complex refractive index $\tilde{n}$ and dielectric function $\varepsilon(\omega)$ such as the reflectivity coefficient R and the attenuation coefficient α. In the fields of photonics, and plasmonics, researchers use the dielectric function in their calculations and investigations [1–8].

2. Modeling of the bulk experimental dielectric function

Here we try to model the experimental dielectric function $\varepsilon^{exp}(\omega)$ of noble metals (Ag and Au) on a wide pulse interval ω with adequate mathematical functions. We consider the measured values of the dielectric function reported by Dold and Mecke [9], Winsemius *et al.* [10], Leveque *et al.* [11], and Thèye *et al.* [12] respectively. These measurements are summarized by Rakiç *et al.* [13] in **Figure 1** (for Ag), and in **Figure 2** (for Au).

2.1 Modeling the experimental dielectric function of bulk Ag

In this part, we will model the real and imaginary parts of the experimental dielectric function of Ag (**Figure 1**). For this we will divide the values of the pulsation ω into several intervals in order to allow us to determine the best fit to suitable mathematical functions over a certain interval. All the results will be presented in **Tables 1–8**.
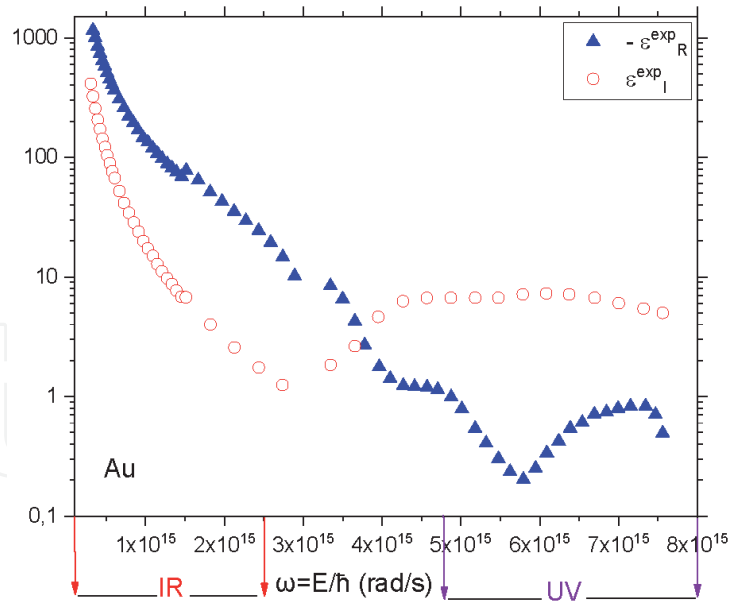
2.1.1 Modeling the real part of the bulk dielectric function of Silver $\varepsilon_{R-Ag}^{exp}(\omega)$

For $1,899 \times 10^{14}\ rad/s \leq \omega \leq 1,275 \times 10^{15}\ rad/s$

$$\varepsilon_{R-Ag}^{exp}(\omega) = \varepsilon_{R_0}^0 + A_1\left(1 - e^{-\omega/t_1}\right) + A_2\left(1 - e^{-\omega/t_2}\right) \tag{4}$$
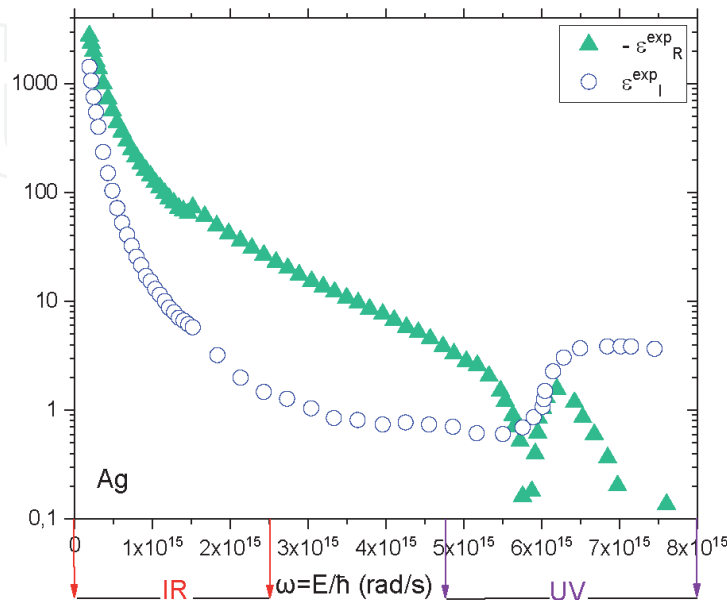
Figure 1.
Real part (▲) and imaginary part (○) of the dielectric function of bulk Ag ([adapted] with permission from [Ref. [13])© The Optical Society.

Figure 2.
Real part(▲) and imaginary part (○) of the dielectric function of bulk Au([adapted] with permission from [Ref. [13])© The Optical Society.

Parameter	$\varepsilon_{R_0}^0$	A_1	$t_1 (\text{rad/s})$	A_2	$t_2 (\text{rad/s})$	R-Square (COD)
Value	10499.713	−1300.876	3.813×10^{14}	−9163.320	1.217×10^{14}	0.9999

Table 1.
Values of the model parameters.

Parameter	$\varepsilon_{R_0}^1$	A_1'	$t_1' (\text{rad/s})$	A_2'	$t_2' (\text{rad/s})$	A_3	$t_3 (\text{rad/s})$	R-Square (COD)
Value	0.305	83.392	1.091×10^{15}	86.023	1.091×10^{15}	86.639	1.091×10^{15}	0,99101

Table 2.
Values of the model parameters.

Parameter	$\varepsilon_{R_0}^2$	A_1''	$t_1'' (\text{rad/s})$	A_2''	$t_2'' (\text{rad/s})$	R-Square (COD)
Value	5.281	−0.006	-9.588×10^{14}	−0.006	-9.576×10^{14}	0.99671

Table 3.
Values of the model parameters.

Parameter	$\varepsilon_{R_0}^3$	A	$\omega_C (\text{rad/s})$	$B (\text{rad/s})$	R-Square (COD)
Value	0.868	0.735	-9.816×10^{14}	3.483×10^{14}	0.96592

Table 4.
Values of the model parameters.

Parameter	$\varepsilon_{R_0}^4$	$\omega_{C'} (\text{rad/s})$	H	$\omega_1 (\text{rad/s})$	$\omega_2 (\text{rad/s})$	R-Square (COD)
Value	2.539	7.140×10^{15}	−2.399	6.978×10^{14}	3.783×10^{24}	0.99613

Table 5.
Values of the model parameters.

3

Parameter	$\varepsilon_{I_0}^0$	B_1	ω_0 (rad/s)	V_1 (rad/s)	R-Square (COD)
Value	−23218.730	585.784	2.267×10^{14}	6.910×10^{13}	0.99998
	B_2	V_2 (rad/s)	B_3	V_3 (rad/s)	
	306.100	1.844×10^{14}	23235.380	2.514×10^{18}	

Table 6.
Values of the model parameters.

Parameter	$\varepsilon_{I_0}^1$	B'	TD (rad/s)	τ (rad/s)	R-Square (COD)
Value	7.076	−6.327	1.38101×10^{15}	4.92416×10^{14}	0.9983

Table 7.
Values of the model parameters.

Parameter	B'_1	B'_2	p	$Ln\omega_{01}$ (rad/s)	h_1 (rad/s)$^{-1}$	$Ln\omega_{02}$ (rad/s)
Value	1.278	1.633	−8.811	9.897×10^{15}	1.262×10^{-16}	6.159×10^{15}
	h_2 (rad/s)$^{-1}$	R-Square (COD)				
	3.945×10^{-15}	0.99733				

Table 8.
Values of the model parameters.

For $1,275 \times 10^{15} \ rad/s \leq \omega \leq 4,873 \times 10^{15} \ rad/s$

$$\varepsilon_{R-Ag}^{exp}(\omega) = A'_1 e^{-\omega/t'_1} + A'_2 e^{-\omega/t'_2} + A_3 e^{-\omega/t_3} + \varepsilon_{R_0}^1 \tag{5}$$

For $4.873 \times 10^{15} \ rad/s \leq \omega \leq 5.650 \times 10^{15} \ rad/s$

$$\varepsilon_{R-Ag}^{exp}(\omega) = A''_1 e^{-\omega/t''_1} + A''_2 e^{-\omega/t''_2} + \varepsilon_{R_0}^2 \tag{6}$$

For $5.650 \times 10^{15} \ rad/s \leq \omega \leq 6.198 \times 10^{15} \ rad/s$

$$\varepsilon_{R-Ag}^{exp}(\omega) = \varepsilon_{R_0}^3 + A \sin\left(\pi \frac{\omega - \omega_C}{B}\right) \tag{7}$$

For $6.198 \times 10^{15} \ rad/s \leq \omega \leq 7.605 \times 10^{15} \ rad/s$

$$\begin{cases} \varepsilon_{R-Ag}^{exp}(\omega) = \varepsilon_{R_0}^4 + H e^{-\frac{1}{2}\left(\frac{\omega - \omega_{C'}}{\omega_1}\right)^2} for(\omega < \omega_{C'}) \\ \varepsilon_{R-Ag}^{exp}(\omega) = \varepsilon_{R_0}^4 + H e^{-\frac{1}{2}\left(\frac{\omega - \omega_{C'}}{\omega_2}\right)^2} for(\omega \geq \omega_{C'}) \end{cases} \tag{8}$$

2.1.2 Modeling the imaginary part of the bulk dielectric function of Silver $\varepsilon_{I-Ag}^{exp}(\omega)$

For $1,900 \times 10^{14} rad/s \leq \omega \leq 1,340 \times 10^{15} rad/s$

$$\varepsilon_{I-Ag}^{exp}(\omega) = \varepsilon_{I_0}^0 + B_1 e^{-(\omega - \omega_0)/V_1} + B_2 e^{-(\omega - \omega_0)/V_2} + B_3 e^{-(\omega - \omega_0)/V_3} \tag{9}$$

For $1.340 \times 10^{15} rad/s \leq \omega \leq 4.251 \times 10^{15} rad/s$

$$\begin{cases} \varepsilon_{I-Ag}^{exp}(\omega) = \varepsilon_{I_0}^1 \, for \, (\omega < TD) \\ \varepsilon_{I-Ag}^{exp}(\omega) = \varepsilon_{I_0}^1 + B'\left(1 - e^{-\frac{(\omega-TD)}{\tau}}\right) for \, (\omega \geq TD) \end{cases} \tag{10}$$

For $4.252 \times 10^{15} rad/s \leq \omega \leq 7.453 \times 10^{15} rad/s$

$$\varepsilon_{I-Ag}^{exp}(\omega) = B_1' + \left(B_2' - B_1'\right)\left[\frac{p}{1 + 10^{(Ln\omega_{01}-\omega)h_1}} + \frac{1-p}{1 + 10^{(Ln\omega_{02}-\omega)h_2}}\right] \tag{11}$$

2.2 Modeling the experimental dielectric function of bulk Au

In this section, we will model the real and imaginary parts of the experimental dielectric function of bulk Au (**Figure 2**). For this we will proceed in the same way as for bulk Ag by dividing the values of the pulsation ω into various intervals. All the results are listed in **Tables 9–15**.

2.2.1 Modeling the real part ofthe bulk dielectric function of Gold $\varepsilon_{R-Au}^{exp}(\omega)$

For $3.319 \times 10^{14} rad/s \leq \omega \leq 1.515 \times 10^{15} rad/s$

$$\varepsilon_{R-Au}^{exp}(\omega) = a_0 + a_1\omega + a_2\omega^2 + a_3\omega^3 + a_4\omega^4 + a_5\omega^5 + a_6\omega^6 + a_7\omega^7 + a_8\omega^8 + a_9\omega^9 \tag{12}$$

For $1.515 \times 10^{15} rad/s \leq \omega \leq 3.345 \times 10^{15} rad/s$

$$\varepsilon_{R-Au}^{exp}(\omega) = a_1' + \left(a_2' - a_1'\right)\left[\frac{q}{1 + 10^{(Ln\omega'_{01}-\omega)g_1}} + \frac{1-q}{1 + 10^{(Ln\omega'_{02}-\omega)g_2}}\right] \tag{13}$$

For $3.345 \times 10^{15} rad/s \leq \omega \leq 4.271 \times 10^{15} rad/s$

$$\varepsilon_{R-Au}^{exp}(\omega) = b_0 + b_1\omega + b_2\omega^2 + b_3\omega^3 + b_4\omega^4 + b_5\omega^5 \tag{14}$$

For $4.271 \times 10^{15} rad/s \leq \omega \leq 7.560 \times 10^{15} rad/s$

$$\varepsilon_{R-Au}^{exp}(\omega) = c_0 + c_1\omega + c_2\omega^2 + c_3\omega^3 + c_4\omega^4 + c_5\omega^5 + c_6\omega^6 + c_7\omega^7 + c_8\omega^8 + c_9\omega^9 \tag{15}$$

2.2.2 Modeling the imaginary part ofthe bulk dielectric function of Gold $\varepsilon_{I-Au}^{exp}(\omega)$

For $3.047 \times 10^{14} rad/s \leq \omega \leq 1.511 \times 10^{15} rad/s$

$$\varepsilon_{I-Au}^{exp}(\omega) = d_0 + d_1\omega + d_2\omega^2 + d_3\omega^3 + d_4\omega^4 + d_5\omega^5 + d_6\omega^6 + d_7\omega^7 + d_8\omega^8 + d_9\omega^9 \tag{16}$$

For $1.511 \times 10^{15} rad/s \leq \omega \leq 4.265 \times 10^{15} rad/s$

$$\varepsilon_{R-Au}^{exp}(\omega) = f_0 + f_1\omega + f_2\omega^2 + f_3\omega^3 + f_4\omega^4 + f_5\omega^5 \tag{17}$$

Parameter	a_0	a_1 $(rad/s)^{-1}$	$a_2(rad/s)^{-2}$	a_3 $(rad/s)^{-3}$	a_4 $(rad/s)^{-4}$	R-Square (COD)
Value	**4835.830**	-8.633×10^{-12}	-6.930×10^{-26}	3.779×10^{-40}	-8.746×10^{-55}	
	a_5 $(rad/s)^{-5}$	a_6 $(rad/s)^{-6}$	a_7 $(rad/s)^{-7}$	a_8 $(rad/s)^{-8}$	a_9 $(rad/s)^{-9}$	0.9999
	1.170×10^{-69}	-9.674×10^{-85}	4.893×10^{-100}	-1.392×10^{-115}	1.710×10^{-131}	

Table 9.
Values of the model parameters.

Parameter	a'_1	a'_2	q	$Ln\omega'_{01}$ (rad/s)	g_1 $(rad/s)^{-1}$	$Ln\omega'_{02}$ (rad/s)	g_2 $(rad/s)^{-1}$	R-Square (COD)
Value	7.786	138.106	0.896	1.495×10^{15}	-1.388×10^{-15}	2.641×10^{15}	-3.366×10^{-15}	0.9996

Table 10.
Values of the model parameters.

Parameter	b_0	b_1 $(rad/s)^{-1}$	b_2 $(rad/s)^{-2}$	b_3 $(rad/s)^{-3}$	b_4 $(rad/s)^{-4}$	b_5 $(rad/s)^{-5}$	R-Square (COD)
Value	-50227.482	6.432×10^{-11}	-3.281×10^{-26}	8.338×10^{-42}	-1.056×10^{-57}	5.337×10^{-74}	0.9997

Table 11.
Values of the model parameters.

Parameter	c_0	c_1 $(rad/s)^{-1}$	c_2 $(rad/s)^{-2}$	c_3 $(rad/s)^{-3}$	c_4 $(rad/s)^{-4}$	R-Square (COD)
Value	**271340.234**	-4.224×10^{-10}	2.912×10^{-25}	-1.167×10^{-40}	2.995×10^{-56}	
	c_5 $(rad/s)^{-5}$	c_6 $(rad/s)^{-6}$	c_7 $(rad/s)^{-7}$	c_8 $(rad/s)^{-8}$	c_9 $(rad/s)^{-9}$	0.99872
	-5.112×10^{-72}	5.801×10^{-88}	-4.220×10^{-104}	1.786×10^{-120}	-3.351×10^{-137}	

Table 12.
Values of the model parameters.

Parameter	d_0	d_1 (rad/s)$^{-1}$	d_2 (rad/s)$^{-2}$	d_3 (rad/s)$^{-3}$	d_4 (rad/s)$^{-4}$	R-Square (COD)
Value	9873.897	-9.845×10^{-11}	4.479×10^{-25}	-1.188×10^{-39}	2.002×10^{-54}	
	d_5 (rad/s)$^{-5}$	d_6 (rad/s)$^{-6}$	d_7 (rad/s)$^{-7}$	d_8 (rad/s)$^{-8}$	d_9 (rad/s)$^{-9}$	0.9999
	-2.212×10^{-69}	1.598×10^{-84}	-7.276×10^{-100}	1.895×10^{-115}	-2.152×10^{-131}	

Table 13.
Values of the model parameters.

Parameter	f_0	f_1 (rad/s)$^{-1}$	f_2 (rad/s)$^{-2}$	f_3 (rad/s)$^{-3}$	f_4 (rad/s)$^{-4}$	f_5 (rad/s)$^{-5}$	R-Square (COD)
Value	115.516	-1.891×10^{-13}	1.299×10^{-28}	-4.538×10^{-44}	7.892×10^{-60}	-5.361×10^{-76}	0.9973

Table 14.
Values of the model parameters.

| Parameter	j_0	j_1 (rad/s)$^{-1}$	j_2 (rad/s)$^{-2}$	j_3 (rad/s)$^{-3}$	j_4 (rad/s)$^{-4}$	R-Square (COD)
Value	-53432.059	1.046×10^{-13}	-8.722×10^{-26}	4.106×10^{-41}	-1.210×10^{-56}	
	j_5 (rad/s)$^{-5}$	j_6 (rad/s)$^{-6}$	j_7 (rad/s)$^{-7}$	j_8 (rad/s)$^{-8}$	j_9 (rad/s)$^{-9}$	0.9974
	2.324×10^{-72}	-2.918×10^{-88}	2.316×10^{-104}	-1.056×10^{-120}	2.111×10^{-137}	

Table 15.
Values of the model parameters.

For $4.265 \times 10^{15} \, rad/s \leq \omega \leq 7.560 \times 10^{15} \, rad/s$

$$\varepsilon_{I-Au}^{exp}(\omega) = j_0 + j_1\omega + j_2\omega^2 + j_3\omega^3 + j_4\omega^4 + j_5\omega^5 + j_6\omega^6 + j_7\omega^7 + j_8\omega^8 + j_9\omega^9$$

(18)

All the results of these different models for both bulk Ag and bulk Au are plotted in the following **Figures 3** and **4**.

In both cases, the experimental results can be well fitted by the models of experimental dielectric function in both its real and imaginary parts with mathematical functions with high accuracy.
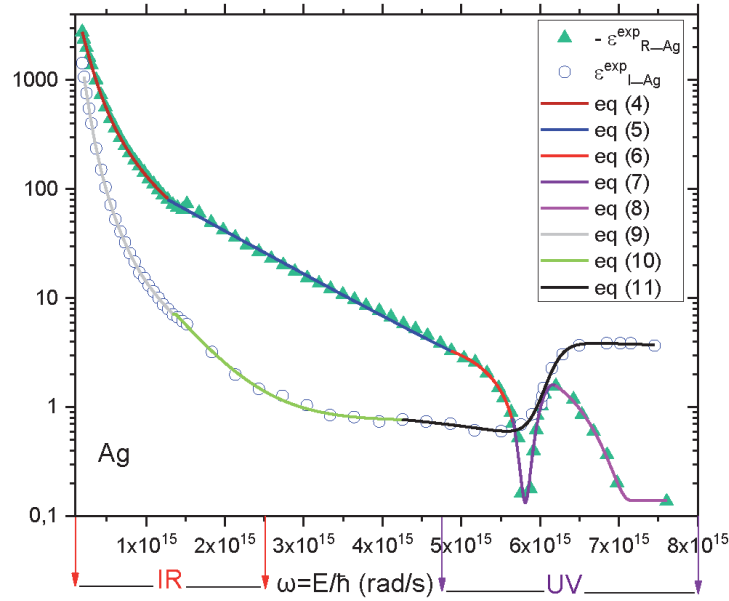
Figure 3.
Real (▲) and imaginary (○) parts of the experimental dielectric function of bulkAg (Ref. [13]). Solid colored curves represent, by pulse intervals, the different mathematical models used in the modeling.
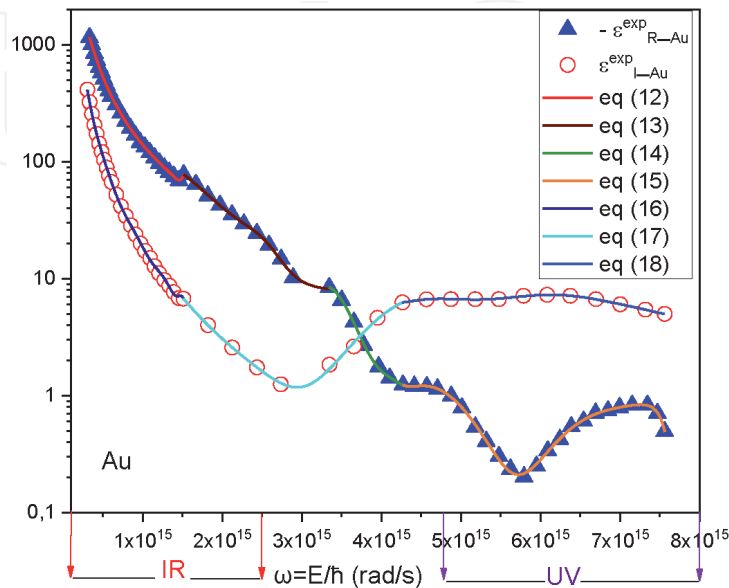
Figure 4.
Real (▲) and imaginary (○) parts of the experimental dielectric function of bulkAu (Ref. [13]). Solid colored curves represent, by pulse intervals, the different mathematical models used in the modeling.

3. Highlighting the contribution of interband and intraband transitions in the expression of dielectric function

In metals, there aretwo types of contribution in the dielectric function, namely contribution of interband transitions denoted $\varepsilon^{iB}(\omega)$ and that of the intraband transitions denoted $\varepsilon^{D}(\omega)$. The dielectric function can be written as the sum of two terms

$$\varepsilon(\omega) = \varepsilon^{D}(\omega) + \varepsilon^{iB}(\omega) \tag{19}$$

The first term corresponds to the intraband component of the dielectric function. It is referred to the optical transitions of a free electron from the conduction band to a higher energy level of the same band. The second term corresponds to the interband component of the dielectric constant. It is referred to optical transitions between the valence bands (mainly d band and s-p conduction bands). Due to Pauli's exclusion principle, an electron from a valence band can only be excited to the conduction band. There is therefore an energy threshold E^{IB} for interband transitions which is placed in the visible band for Au and near the UV region for Ag. This component is often overlooked in the infrared range (this is valid only for alkali metals) where the optical response is dominated by intraband absorption. This type of transitions dominates the optical response beyond E^{IB}.

The intraband part $\varepsilon^{D}(\omega)$ of the dielectric function is described by the well-known free-electronorDrude Model [14]:

$$\varepsilon^{D}(\omega) = 1 - \frac{\omega_p^2}{\omega(\omega + i\gamma)} \tag{20}$$

where γ is the collision rate (probability of collision per unit of time). $\varepsilon\omega = \varepsilon1\omega + i\varepsilon2\omega$.

We note that $\gamma = \tau^{-1}$ and τ is the elastic diffusion time

$$\tau = \frac{l_0}{v_f} \tag{21}$$

where l_0 is the mean free path of electrons and v_f is the Fermi speed.

In the Drude model, there appears a pulsation called the plasmon frequency of a bulk metal given by

$$\omega_p = \sqrt{\frac{n_c e^2}{\varepsilon_0 m_{eff}}} \tag{22}$$

Where ε_0 is dielectric constant in vacuum.

The electronic structure of bulk noble metals such as Ag and Au, the respective values of the conduction electron density n_c, the effective mass m_{eff}, the Fermi speed v_f conduction electrons and the mean free path of electron l_0, are listed in the following **Table 16** [15]:

3.1 Contribution of intraband transitions to dielectric function

The intraband dielectric function described by the Drude model [14] as denoted $\varepsilon^{D}(\omega)$ can be written as

Metal	n_c $(\times 10^{28} m^{-3})$	$\frac{m_{\text{eff}}}{m_e}$	v_f (nm/fs)	l_0 (nm)
Ag	5.86	0.96	1.39	55
Au	5.90	0.99	1.40	42

From Phys. Review B. **6.** *4376(1972).*

Table 16.
Electronic properties of Ag and Au.

$$\varepsilon^D(\omega) = \varepsilon_R^D(\omega) + i\varepsilon_I^D(\omega) \tag{23}$$

The real and imaginary parts of the relative dielectric function (intraband) are written as follows

$$\varepsilon_R^D(\omega) = 1 - \frac{\omega_p^2}{\omega^2 + \gamma^2} \tag{24}$$

$$\varepsilon_I^D(\omega) = \frac{\omega_p^2 \gamma}{\omega(\omega^2 + \gamma^2)} \tag{25}$$

Usually, for noble metals $\omega \gg \gamma$ in the near UV range and up to the near IR, we can write

$$\varepsilon_R^D(\omega) = 1 - \frac{\omega_p^2}{\omega^2} \tag{26}$$

$$\varepsilon_I^D(\omega) = \frac{\omega_p^2 \gamma}{\omega^3} \tag{27}$$

The following **Table 17** shows the values of plasma frequencies and the collision rate of noble metals (Gold, Silver):

The results of the calculations of the contribution of intraband effects to dielectric function are represented in their real and imaginary parts for bulk Ag (**Figure 5**) and for bulk Au (**Figure 6**).

For the noble metals (Gold, Silver), we observed that the real and imaginary parts decrease with increasing pulsation. The further away from the pulsations corresponding to IR radiation and the closer we get to the pulsations corresponding to UV radiation, these values decrease.

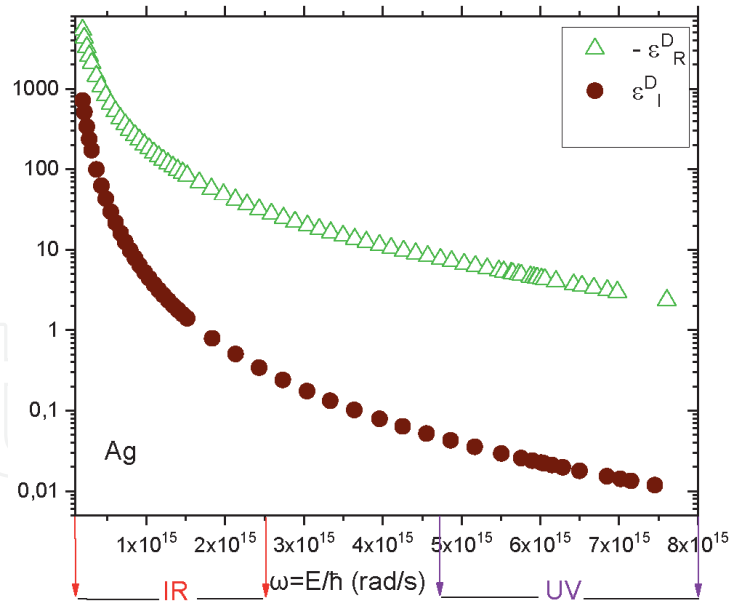## 3.2 Contribution of interband transitions to dielectric function

The interband dielectric function denoted $\varepsilon^{iB}(\omega)$ is described by the following term

$$\varepsilon^{iB}(\omega) = \varepsilon_R^{iB}(\omega) + i\varepsilon_I^{iB}(\omega) \tag{28}$$
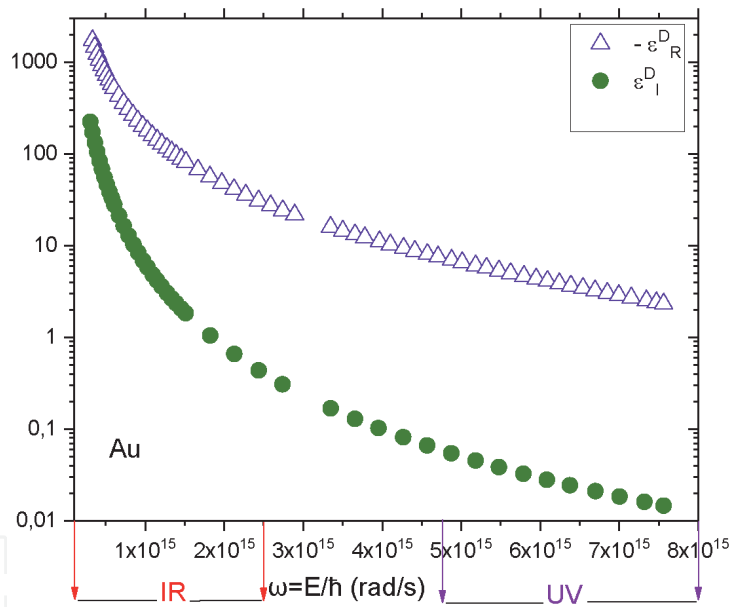
Metal	ω_p^2 (rad/s)^2	γ (s^{-1})
Ag	1.9428×10^{32}	2.5273×10^{13}
Au	1.8968×10^{32}	3.3333×10^{13}

Table 17.
Plasma frequency and collision rate values for Ag and Au.

Figure 5.
Real (△) imaginary part (●) of the intraband dielectric function of bulk Ag.

Figure 6.
Real (△) imaginary part (●) of intraband dielectric function of bulk Au.

The real and imaginary parts of the interband dielectric function are written respectively as follows:

$$\varepsilon_R^{iB}(\omega) = \varepsilon_R^{exp}(\omega) - \varepsilon_R^{D}(\omega) \tag{29}$$

$$\varepsilon_I^{iB}(\omega) = \varepsilon_I^{exp}(\omega) - \varepsilon_I^{D}(\omega) \tag{30}$$

where

$$\varepsilon^{exp}(\omega) = \varepsilon_R^{exp}(\omega) + i\varepsilon_I^{exp}(\omega) \tag{31}$$

Here $\varepsilon^{exp}(\omega)$, $\varepsilon_R^{exp}(\omega)$, and $\varepsilon_I^{exp}(\omega)$ are the experimental values, real and imaginary parts of the complex dielectric function, respectively.

The results of the calculations of the contribution of interband transitions to real and imaginary parts of dielectric function are represented respectively for bulk Ag (**Figure 7**) and for bulk Au (**Figure 8**).

As shown in **Figure 7**, the real part of the contribution of interband effects to the dielectric function of bulk Ag decreases with increasing pulsation in the IR radiation domain then is still almost constant with small variations from $\omega = 1.5 \times 10^{15} \text{rad/s}$ and this until the end of the UV radiation range. Concerning the imaginary part of this contribution, it is almost less important than the real part. It decreases with increasing pulsation in the range corresponding to IR radiation, then varies very little to the value of the pulsation $\omega = 6 \times 10^{15} \text{rad/s}$ in the range of UV radiation, in this area increase from 0.4 to 1.4 and finally remains constant for the rest of the UV pulses. The imaginary part becomes superior to the real part for UV pulses higher than the value $\omega = 6 \times 10^{15} \text{rad/s}$.
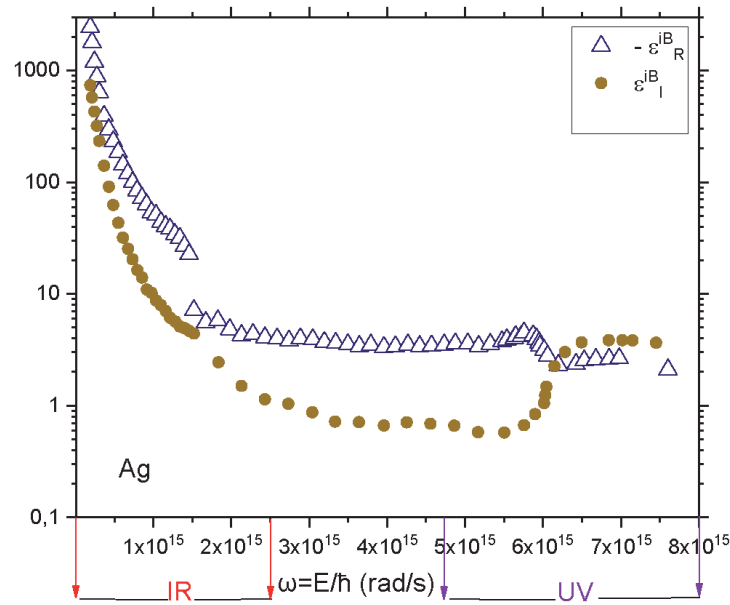
Figure 7.
Real ($\triangle$) and imaginary part ($\bullet$) of the interband dielectric function of bulk Ag.
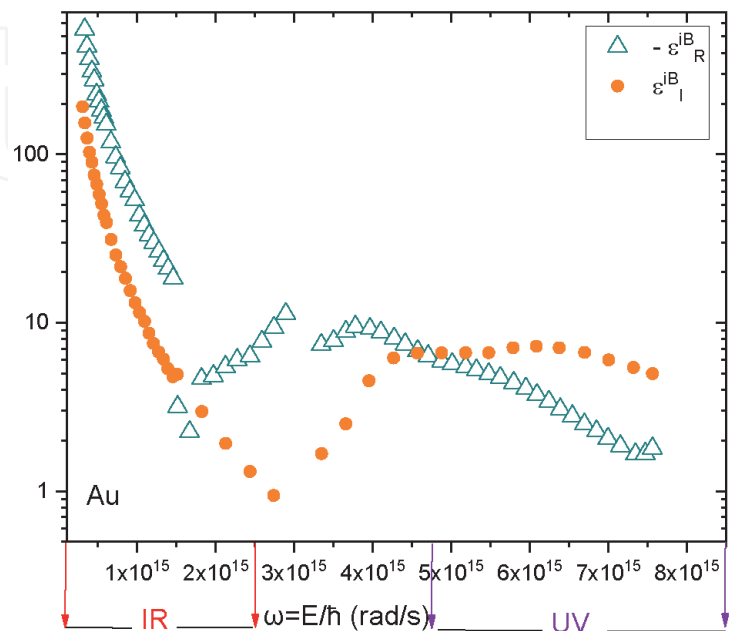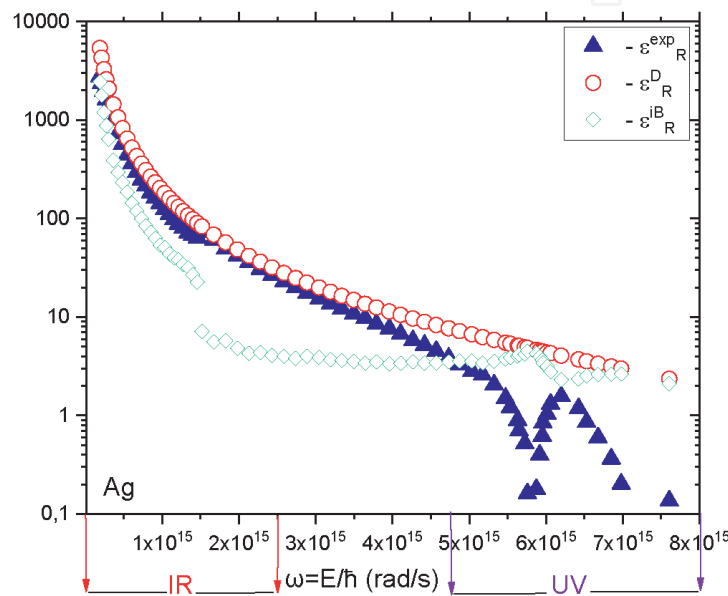

Figure 8.
Real ($\triangle$) and imaginary part ($\bullet$) of the interband dielectric function of bulk Au.

We note that for Gold, the real and imaginary parts of the contribution of interband transitions decrease by increasing the values of the pulses in the IR domain to the value $\omega = 4.5 \times 10^{15}$rad/s with a real part almost higher than the imaginary part. For pulsation values in the UV range above the value $\omega = 4.5 \times 10^{15}$rad/s, with a slight variation the imaginary part becomes superior to the real part.

In **Figures 9** and **10** (for Ag) and **Figures 11** and **12** (for Au), we have presented experimental values, the contributions of intraband and interband transitions to the real and imaginary parts of the dielectric function.

Concerning the real part, we note that, the real part due to the intraband transitions noted $\varepsilon_R^D(\omega)$ is in very good agreement with the experimental values in the full domain corresponding to IR radiation and up to the value $\omega = 4 \times 10^{15}$rad/s. In this range of pulsations, we can conclude that the participation in the dielectric function

Figure 9.
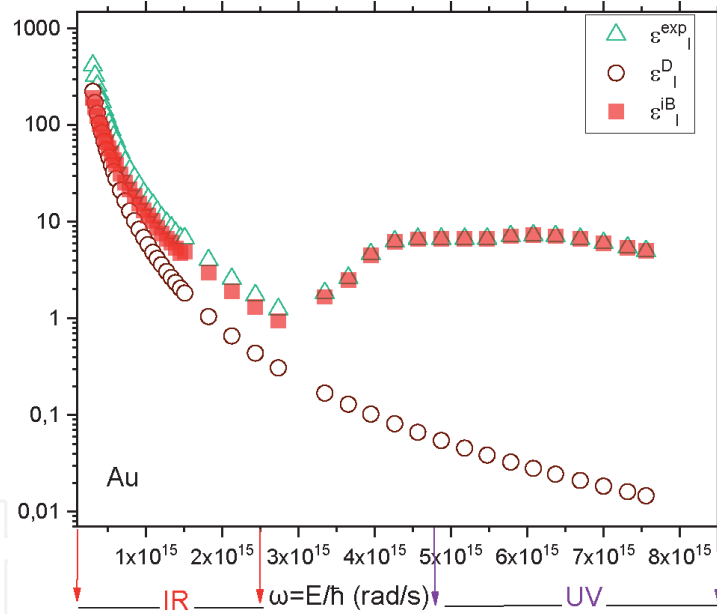*Real parts of the dielectric function of Ag: experimental values (▲) ([Ref. [13]]), intraband transitions (○), interband transitions (◇).*
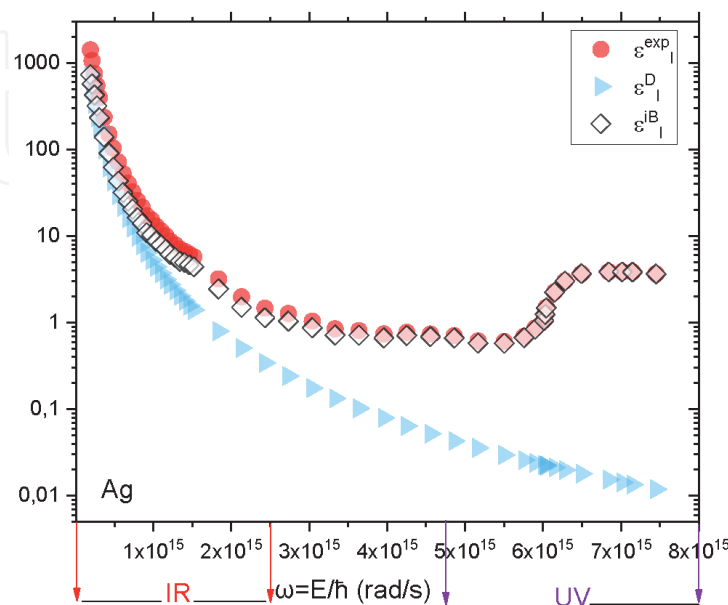
Figure 10.
Imaginary parts of the dielectric function of Ag: experimental values (●) ([Ref. [13]]), intraband transitions (▶), interband transitions (◇).
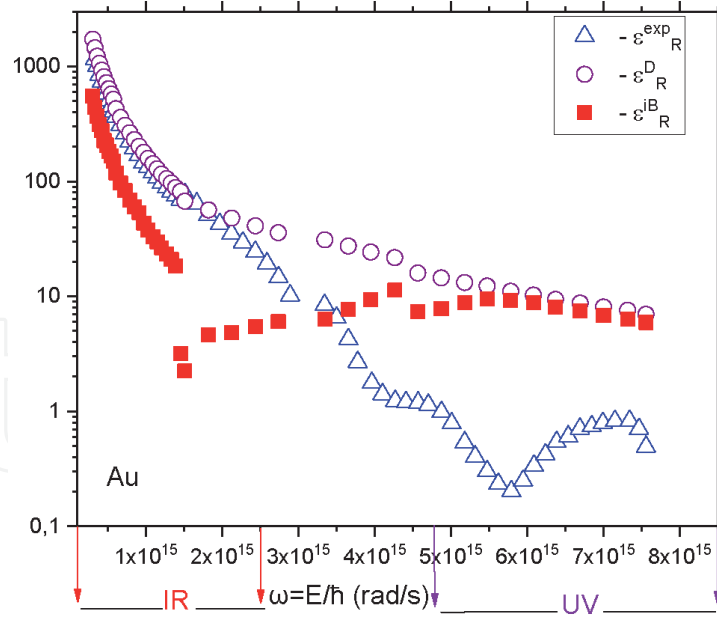
Figure 11.
Real parts of the dielectric function of Au: experimental values (△) ([Ref. [13]]), intraband transitions (○),
interband transitions (■).

Figure 12.
Imaginary parts of the dielectric function of Au: experimental values (△) ([Ref. [13]]), intraband transitions
(○),interband transitions (■).

due to inter-band transitions is negligible compared to that of intra-band transitions. For $\omega > 4.5 \times 10^{15}\,rad/s$ in the range of UV radiation, the two contributions due to intraband and interband transitions are equivalent but differ from the experimental measurements.

Concerning the imaginary part, we note that the imaginary part due to the interband transitions noted $\varepsilon_I^{iB}(\omega)$ is practically confused with the imaginary experimental part in the whole field of pulsations from the IR domain to the end of the UV domain. This indicates that the imaginary part due to intraband transitions is negligible compared to the imaginary part due to interband transitions.

For Gold, we note that, the real part due to the intraband transitions noted $\varepsilon_R^D(\omega)$ is in very good agreement with the real experimental values in the whole range

corresponding to IR radiation and up to the value $\omega = 2 \times 10^{15}$rad/s. In this range of pulsations, we can conclude that the participation in the dielectric function due to interband transitions is negligible compared to that of intraband transitions. For $\omega > 2 \times 10^{15}$rad/s and up to the UV radiation domain, the two contributions due to intraband and interband transitions differ significantly from the experimental measurements. These two contributions are very similar in the field of UV for $\omega \geq 2.5 \times 10^{15}$rad/s.

Concerning the imaginary part, as for Silver, we see that the imaginary part due to the interband transitions noted $\varepsilon_I^{iB}(\omega)$ is practically confused with the imaginary experimental part in the whole field of pulsations from the IR domain to the end of the UV domain. This indicates that the imaginary part due to intraband transitions is negligible compared to the imaginary part due to interband transitions.

4. Modeling the dielectric functions of nanometri cAg and nanometric Au

In this section, we study the dielectric functions of nanometric Ag and nanometric Au. They are composed of a few tens to several thousand atoms. Their very small characteristic dimensions, in the nanometer range (i.e. well under optical wavelengths), give rise to extraordinary electronic and optical properties that cannot be observed in bulk materials. These properties are clearly influenced by the size, form of the nanoparticle and the nature of the host environment. We consider the measured values of dielectric function used in the previous paragraphs, and try to model those using theoretical models for nanometals such as the Drude Lorentz (DL) model, the Drude two-point critical model DCP and the Drude three-point critical model DCP3.

The optical properties of metallic nanoparticles are dominated by the collective oscillation of conduction electrons induced by interaction with electromagnetic radiation (IR, UV).

The collective excitation of nanoparticle conduction electrons gives them new optical properties; we consider the following two effects:

- Plasmons guided along a metallic film of nanometric cross-section (1D confinement).

- Surface plasmons located in a metallic particle of nanometric size (0D confinement).

4.1 Drude Lorentz (DL) model

For the study of resonant nanostructures, it is important to have a good description of the permittivity of the metal in a large frequency band. For this purpose, the validity band of the Drude Model is often extended by adding Lorentzian terms [16] depending in the following form

$$\varepsilon_{DL}(\omega) = \varepsilon_\infty - \frac{\omega_D^2}{\omega^2 + i\gamma\omega} + \sum_{l=1}^{2} \frac{f_l \Omega_l^2}{\Omega_l^2 - \omega^2 - i\Gamma_l\omega} \qquad (32)$$

The dielectric function described by the Drude Lorentz model is written as follows

$$\varepsilon_{DL}(\omega) = \varepsilon_{DL}^R(\omega) + i\varepsilon_{DL}^{im}(\omega) \qquad (33)$$

where:
The real part of the dielectric function according to the DL model

$$\varepsilon_{DL}^R(\omega) = \varepsilon_\infty - \frac{\omega_D^2}{\omega^2 + \gamma^2} + \frac{f_1\Omega_1^2(\Omega_1^2 - \omega^2)}{(\Omega_1^2 - \omega^2)^2 + (\Gamma_1\omega)^2} + \frac{f_2\Omega_2^2(\Omega_2^2 - \omega^2)}{(\Omega_2^2 - \omega^2)^2 + (\Gamma_2\omega)^2} \quad (34)$$

The imaginary part of the dielectric function according to the DL model:

$$\varepsilon_{DL}^{im}(\omega) = \frac{\gamma\omega_D^2}{\omega^3 + \gamma^2\omega} + \frac{f_1\Omega_1^2\Gamma_1\omega}{(\Omega_1^2 - \omega^2)^2 + (\Gamma_1\omega)^2} + \frac{f_2\Omega_2^2\Gamma_2\omega}{(\Omega_2^2 - \omega^2)^2 + (\Gamma_2\omega)^2} \quad (35)$$

The studies of Vial and Laroche [16] on the permittivity of Auand Ag metals used in their model with the parameters are listed in **Table 18**.

The results of modeling the experimental dielectric function in its real and imaginary parts using the DL model are shown in **Figures 13** and **14** for Au(in **Figures 15** and **16** for Ag).

4.2 Drude model with two critical points DCP

In order to describe the metal in the largest possible range of pulsations, another formula describing the two-point critical Drude model (DCP) [16] will appear in this paragraph.

The dielectric function of Au and Ag is can be expressed from as [17]:

$$\varepsilon_{DCP}(\omega) = \varepsilon_\infty - \frac{\omega_D^2}{\omega^2 + i\gamma\omega} + \sum_{l=1}^{2} A_l\Omega_l\left[\frac{e^{i\phi}}{\Omega_l - \omega - i\Gamma_l} + \frac{e^{-i\phi}}{\Omega_l + \omega + i\Gamma_l}\right] \quad (36)$$

The dielectric function described by the Drude two-critical-point model is written as follows

$$\varepsilon_{DCP}(\omega) = \varepsilon_{DCP}^R(\omega) + i\varepsilon_{DCP}^{im}(\omega) \quad (37)$$

where
The real part of the dielectric function according to the DCP model:

|	ε_∞	ω_D (rad/s)	γ (rad/s)	f_1	
Au	6.2137	1.3323×10^{16}	1.3235×10^{14}	3.4620	
Ag	1.7984	1.3359×10^{16}	8.7167×10^{13}	3.0079	
	Ω_1 (rad/s)	Γ_1 (rad/s)	f_2	Ω_2 (rad/s)	Γ_2 (rad/s)
Au	4.7914×10^{15}	2.1367×10^{15}	-3.4886	4.2111×10^{14}	4.5572×10^{17}
Ag	8.1635×10^{15}	4.3785×10^{17}	2.3410	3.8316×10^{16}	6.0574×10^{16}

*From J. Phys. D. Appl. Phys. **40**,7154 (2007).*

Table 18.
Optimized parameters of the Drude Lorentz model for noble metals (Au and Ag).
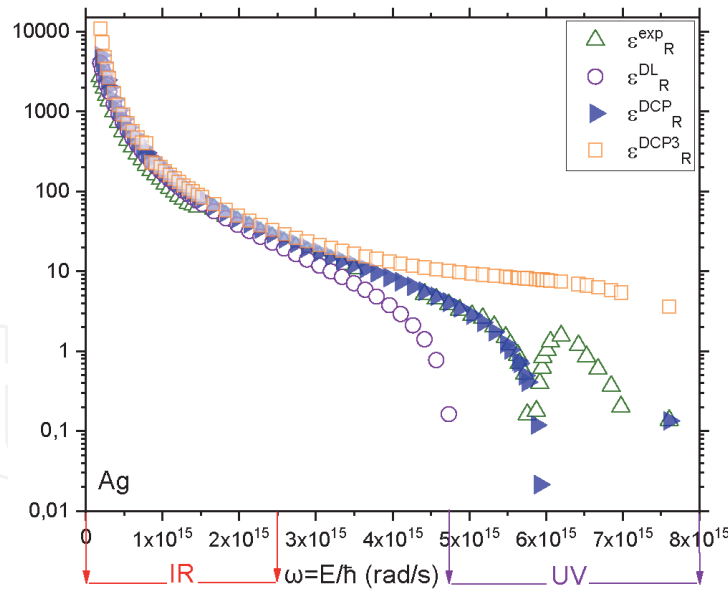
Figure 13.
Real part of the dielectric function of nanometric Ag: experimental values (△) ([Ref. [13]]), the DL model (○), the DCP model (▶) and the DCP3model (□).
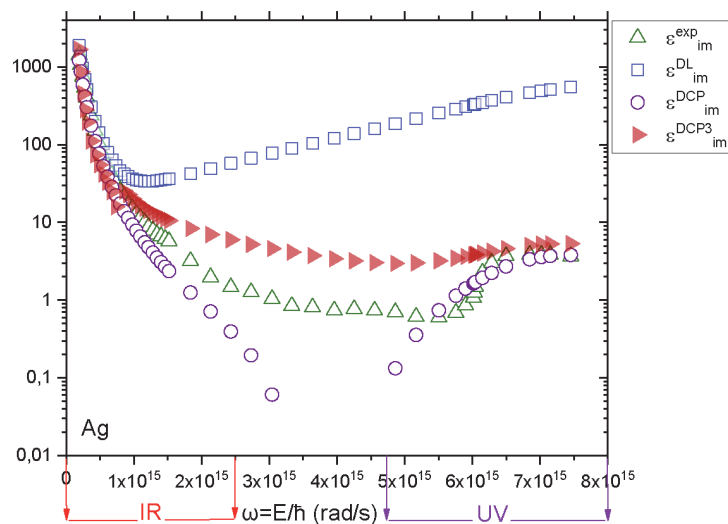
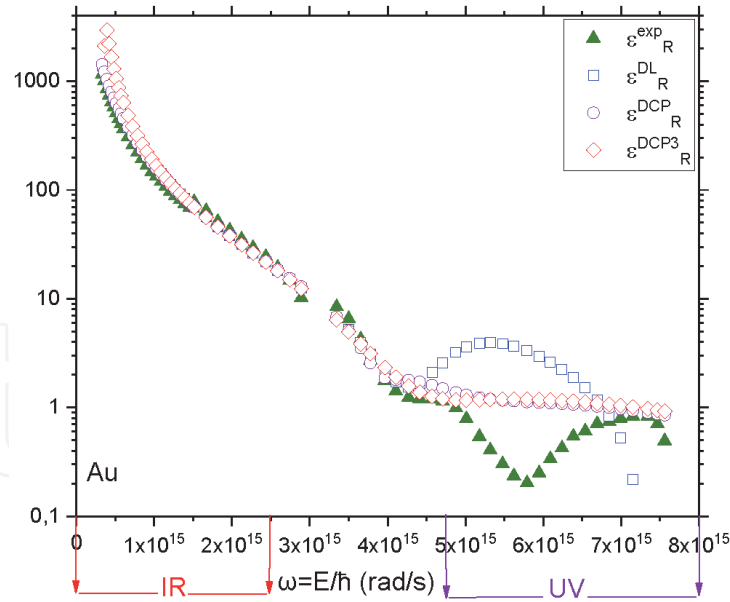**Figure 14.**
Imaginary part of the dielectric function of nanometric Ag:experimental values (△) ([Ref. [13]]), the DL model (□), the DCPmodel (○), and the DCP3 model (▶).

$$\varepsilon_{DCP}^{R}(\omega) = \varepsilon_{\infty} - \frac{\omega_D^2}{\omega^2 + \gamma^2}$$
$$+ \sum_{l=1}^{2} A_l \Omega_l \left[\frac{(\Omega_l - \omega) \cos \phi_l - \Gamma_l \sin \phi_l}{(\Omega_l - \omega)^2 + \Gamma_l^2} + \frac{(\Omega_l + \omega) \cos \phi_l - \Gamma_l \sin \phi_l}{(\Omega_l + \omega)^2 + \Gamma_l^2} \right]$$
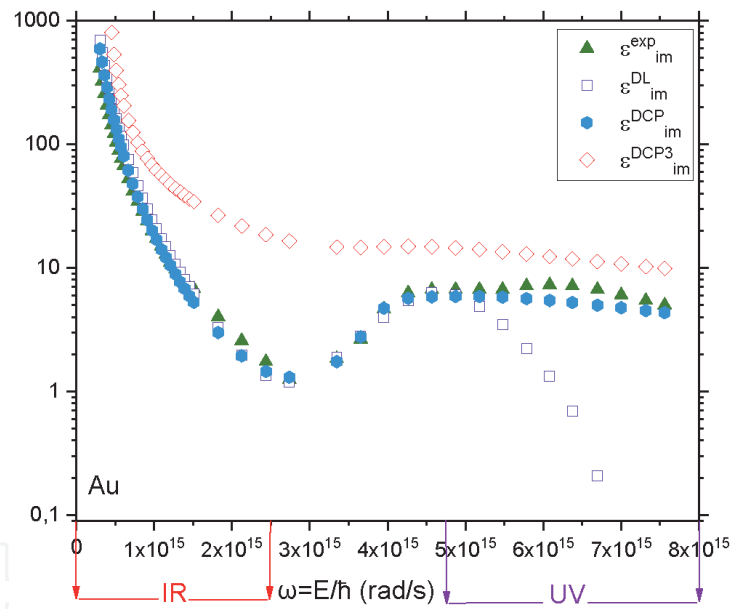
(38)

The imaginary part of the dielectric function according to the DCP model:

$$\varepsilon_{DCP}^{im}(\omega) = \frac{\gamma \omega_D^2}{\omega^3 + \gamma^2 \omega}$$
$$+ \sum_{l=1}^{2} A_l \Omega_l \left[\frac{(\Omega_l - \omega) \sin \phi_l + \Gamma_l \cos \phi_l}{(\Omega_l - \omega)^2 + \Gamma_l^2} + \frac{(\Omega_l + \omega) \sin \phi_l - \Gamma_l \cos \phi_l}{(\Omega_l + \omega)^2 + \Gamma_l^2} \right]$$

(39)

Figure 15.
Real part of the dielectric function of nanometric Au: experimental values (▲) ([Ref. [13]), the DLmodel (▫), the DCP model (○), and the DCP3 model (◇).

Figure 16.
Imaginary part of dielectric of nanometric Au: experimental values (▲) ([Ref. [13]), the DL model (▫), the DCP model (●), and theDCP3 model (◇).

The work of Alexandre Vial's [17] on the permittivity of the noble metals (Gold, Silver) made model with the parameters are listed in **Table 19**.

The results of modeling the experimental dielectric function in its real and imaginary parts using the Drude two-point DCP critical point model are shown in **Figures 13** and **14** for Au (in **Figures 15** and **16** for Ag).

4.3 Drude model with three critical points DCP3

The DCP3 model describes the response of the dielectric function in a wider pulsation band, it should be noted that the DCP3 model gives a very good description of the dielectric function of noble metals; it is expressed by the relation [18]:

	ε_∞	ω_D (rad/s)	γ (rad/s)	A_1	ϕ_1 (rad)	Ω_1 (rad/s)
Au	1.1431	1.3202×10^{16}	1.0805×10^{14}	0.26698	−1.2371	3.8711×10^{15}
Ag	15.833	1.3861×10^{16}	4.5841×10^{13}	1.0171	−0.93935	6.6327×10^{15}

	A_2	ϕ_2 (rad)	Ω_2 (rad/s)	Γ_2 (rad/s)	Γ_1 (rad/s)
Au	3.0834	−1.0968	4.1684×10^{15}	2.3555×10^{15}	4.4642×10^{14}
Ag	15.797	1.8087	9.2726×10^{17}	2.3716×10^{17}	1.6666×10^{15}

From Appl. Phys.B 93, 140 (2008).

Table 19.
Optimized parameters of the Drude two-point critical point model DCP, dielectric function for noble metals (Gold, Silver).

$$\varepsilon_{DCP3}(\omega) = \varepsilon_\infty + \frac{\sigma/\varepsilon_0}{i\omega} + \sum_{l=1}^{3} A_l\Omega_l \left[\frac{e^{i\phi}}{\Omega_l - \omega - i\Gamma_l} + \frac{e^{-i\phi}}{\Omega_l + \omega + i\Gamma_l} \right] \tag{40}$$

The dielectric function described by the Drude two-critical-point model is written as follows:

$$\varepsilon_{DCP3}(\omega) = \varepsilon^R_{DCP3}(\omega) + i\varepsilon^{im}_{DCP3}(\omega) \tag{41}$$

Where:
The real part of the dielectric function in the DCP3 model:

$$\varepsilon^R_{DCP3}(\omega) = \varepsilon_\infty + \sum_{l=1}^{3} A_l\Omega_l \left[\frac{(\Omega_l - \omega)\cos\phi_l - \Gamma_l \sin\phi_l}{(\Omega_l - \omega)^2 + \Gamma_l^2} + \frac{(\Omega_l + \omega)\cos\phi_l - \Gamma_l \sin\phi_l}{(\Omega_l + \omega)^2 + \Gamma_l^2} \right] \tag{42}$$

The imaginary part of the dielectric function in the DCP3 model:

$$\varepsilon^{im}_{DCP3}(\omega) = \frac{-\sigma/\varepsilon_0}{\omega} + \sum_{l=1}^{3} A_l\Omega_l \left[\frac{(\Omega_l - \omega)\sin\phi_l + \Gamma_l \cos\phi_l}{(\Omega_l - \omega)^2 + \Gamma_l^2} - \frac{(\Omega_l + \omega)\sin\phi_l + \Omega_l \cos\phi_l}{(\Omega_l + \omega)^2 + \Gamma_l^2} \right] \tag{43}$$

The parameters of this model are given in **Table 20**.

The results of modeling the real and imaginary parts of experimental dielectric function using the Drude three-point critical point model DCP3 are shown in **Figures 13** and **14** for Au (in **Figures 15** and **16** for Ag).

Concerning the real part of the dielectric function of nanometric Ag; the model that is very much in agreement with the experiment up to the value of the pulsation $\omega \approx 6 \times 10^{15}$ rad/s, placed in the UV region, is the DCP model. The other models are also valid up to the value of $\omega \approx 3 \times 10^{15}$ rad/s. This interval covers the whole pulsation zone in the IR domain.

For the imaginary part of nanometric Ag, we find that for pulsations located in the IR domain and less than $\omega < 1.5 \times 10^{15}$rad/s, the most appropriate model with experience in this range is the DCP3 model. For pulsation values 1.5×10^{15}rad/s $< \omega < 6 \times 10^{15}$rad/s, the most suitable model to the measured values of the

	ε_∞	σ/ε_0	A_1	ϕ_1 (rad)	Ω_1 (rad/s)	Γ_1 (rad/s)	A_2
Au	1.1156	27.825	0.5548	2.8463	4.506×10^{16}	5.09×10^{16}	679.7606
Ag	1.4783	8.7191	1.007	-0.9621	6.617×10^{15}	1.7415×10^{15}	5377.4512
	ϕ_2 (rad)	Ω_2 (rad/s)	Γ_2 (rad/s)	A_3	ϕ_3 (rad)	Ω_3 (rad/s)	Γ_3 (rad/s)
Au	-0.0998	3.4587×10^{14}	3.064E13	3.5244	4.6586	3.5832×10^{15}	1.68784×10^{15}
Ag	-0.0092	1.3545×10^{14}	6.56505×10^{12}	2.6077	-2.8539	8.1007×10^{14}	8.7193×10^{12}

*From Superlattices and Microstructures **47**, 67 (2009).*

Table 20.
Optimized parameters of Drude at three critical points DCP3 of the dielectric function of noble metals (Au and Ag).

dielectric function is still the DCP3 model. For $\omega > 6 \times 10^{15}$rad/s in the UV range, the two models DCP and DCP3 are very close to the experiment. The DCP3 model is better than the DCP model.

In the case of the real part of the dielectric function of nanometric Au, the DL, DCP, and DCP3 models are all in very good agreement with the experiment up to the value of the pulsation $\omega \approx 5 \times 10^{15}$rad/s; which is the beginning of the UV radiation region. Beyond this value, the three models deviate from the measured values (**Figure 15**). From the value of $\omega \approx 6.75 \times 10^{15}$rad/s two models DCP and DCP3 agree well the experimental values. As shown in **Figure 16**, concerning the imaginary part of the dielectric function of nanometric Au, we note that the DCP model is in excellent agreement with the experiment over the whole domain of pulsation values including values corresponding to both IR and UV radiation. The DL model is also close to the experimental values up to the value $\omega \approx 5 \times 10^{15}$rad/s.

5. Conclusion

In this work, we modeled the dielectric function of noble metals (silver and gold) in their bulk and nanometric states. Initially, we modeled the measured dielectric functions of these two metals using explicit mathematical functions and the results are in very good agreement with the experiment. Moreover, we have decomposed these measured values of the dielectric functions; in their real and imaginary parts; into several intervals according to the pulsations that sweep the domains corresponding to IR and UV radiation via the intermediate values. The obtained results are very conclusive, and depending on the pulsation domain studied, it is possible to use the corresponding mathematical function in simulations and calculations. Then, we highlighted the importance of the contributions of intraband and interband transitions in dielectric function for both Ag and Au. For Ag, we note that the imaginary part of the dielectric function due to interband transitions denoted $\varepsilon_I^{iB}(\omega)$ is almost the same with the imaginary experimental part in the whole field of pulsations from the IR domain to the end of the UV domain. This indicates that the imaginary part due to intraband transitions is negligible compared to the imaginary part due to interband transitions. Concerning the real part of the dielectric function, we note that, the real part due to the intraband transitions noted $\varepsilon_R^D(\omega)$ is in very good agreement with the real experimental values in the entire range corresponding to IR radiation and up to the value $\omega = 4 \times 10^{15}$rad/s. In this range of pulsation, we can conclude that the contribution to the dielectric function due to interband transitions is negligible compared to that of intraband transitions.

In the case of Au, we note that the real part of the dielectric function due for $\omega > 4.5 \times 10^{15}$rad/$s$ and in the field of UV radiation, the two contributions due to intraband and interband transitions are equivalent but they differ from the experiment. to the intraband transitions denoted as $\varepsilon_R^D(\omega)$ is in very good agreement with the real experimental values over the whole range corresponding to IR radiation and up to the value $\omega = 2.5 \times 10^{15}$rad/s. In this range of pulsation, we can conclude that the participation in the dielectric function due to interband transitions is negligible compared to that of intraband transitions. For $\omega > 2.5 \times 10^{15}$rad/$s$ and up to the UV radiation domain, the two contributions due to intraband and interband transitions differ significantly from the experimental results. The two contributions are very similar in the field of UV for $\omega \geq 2.5 \times 10^{15}$rad/s. Concerning the imaginary part, and as for Ag, we note that the imaginary part due to the interband transitions noted $\varepsilon_I^{iB}(\omega)$ is practically the same with the imaginary experimental part in the

whole field of pulsations from the IR domain to the end of the UV domain. This indicates that the imaginary part due to intraband transitions is negligible compared to the imaginary part due to interband transitions.

In the last part of this paper, we have modeled the dielectric functions of Ag and Au, using theoretical models that deal with nanometric systems such as the Drude Lorenz model, the Drude two-point critical model, and the Drude three-point critical model.In the case of nanometic Ag, the real part of the dielectric function model agrees well with the experiment up to the value of the pulsation $\omega \approx 6 \times 10^{15}$rad/s, which is located in the UV radiation region, is the DCP model. The other models are also valid up to the value of $\omega \approx 3 \times 10^{15}$rad/s. This interval covers the entire pulsation zone located in the IR domain. For the imaginary part of Ag, we find that for pulsation located in the IR domain and less than $\omega < 1.5 \text{x} 10^{15}$rad/s, the most appropriate model is the DCP3 model. For pulsation values 1.5×10^{15}rad/s $< \omega < 6 \times 10^{15}$rad/s, model that deviates the least from the measured values of the dielectric function is still the DCP3 model. For $\omega > 6 \times 10^{15}$rad/s in the UV domain, the two models DCP and DCP3 are very close to the experience with a better approach using the DCP3 model.

For nanometric Au, concerning the real part of the dielectric function, the three models DL, DCP, and DCP3 are all in very good agreement with the experiment up to the value of the pulsation $\omega \approx 5 \times 10^{15}$rad/s; which is the beginning of the UV radiation region. Beyond this value, the three models deviate from the experiment. From the value of $\omega \approx 6.75 \times 10^{15}$rad/s the two models DCP and DCP3 meet the experimental values. Concerning the imaginary part, we note that the DCP model is in very good agreement with the experiment on the whole range of pulsation values including values corresponding to both IR and UV radiation. The DL model is also very close to the experimental values up to the value $\omega \approx 5 \times 10^{15}$ rad/s.

Acknowledgements

Author details

Brahim Ait Hammou[1], Abdelhamid El Kaaouachi[1*], Abdellatif El Oujdi[2], Adil Echchelh[2], Said Dlimi[3], Chi-Te Liang[4] and Jamal Hemine[2]

1 Faculty of Sciences of Agadir, Materials and Physicochemistry of the Atmosphere and Climate Group, BP, Agadir, Morocco

2 Faculty of Sciences Ibn Tofail, Laboratory of Energetic Engineering and Materials, Kenitra, Morocco

3 Faculty of Sciences of Agadir, Physics Department, BP, Agadir, Morocco

4 Department of Physics, National Taiwan University, Taipei, Taiwan

*Address all correspondence to: kaaouachi21@yahoo.fr

IntechOpen

References

[1] M. J. Ambrosio and U. Thumm, "Energy-resolved attosecond interferometric photoemission from Ag(111) and Au(111) surfaces," Phys. Rev. A **97**, 043431 (2018).

[2] M. J. Ambrosio and U. Thumm, "Electronic structure effects in spatiotemporally resolved photoemission interferograms of copper surfaces," Phys. Rev. A **96**, 051403(R) (2017).

[3] S. R. Leone, C. W. McCurdy, J. Burgdörfer, L. S. Cederbaum, Z. Chang, N. Dudovich, J. Feist, C. H. Greene, M. Ivanov, R. Kienberger, U. Keller, M. F. Kling, Z.-H. Loh, T. Pfeifer, A. N. Pfeiffer, R. Santra, K. Schafer, A. Stolow, U. Thumm, and M. J. J. Vrakking, "What will it take to observe processes in 'real time'?," Nat. Photon. **8**, 162-166 (2014).

[4] F.Calegari, G. Sansone, S. Stagira, C. Vozzi, and M. Nisoli, "Advances in attosecond science," J. Phys. B **49**, 062001 (2016).

[5] Yanzeng Li, Margaret Kocherga, Serang Park, Marc Lata, Micheal McLamb, Glenn Boreman, Thomas A. Schmedake, and Tino Hofmann, "Optical dielectric function of Si(2,6-bis (benzimidazol-2′-yl)pyridine)$_2$ determined by spectroscopic ellipsometry," Opt. Mater. Express 9, 3469–3475 (2019).

[6] M. J. Ambrosio and U. Thumm, "Comparative time-resolved photoemission from the Cu(100) and Cu(111)," surfaces Phys. Rev. A 94, 063424 (2016).

[7] N. Manrique and H. Riascos, "Estimation of Dielectric Constant and Thickness of Copper Thin Films Using Surface Plasmon Resonance," in *Latin America Optics and Photonics Conference*, OSA Technical Digest (Optical Society of America, 2018), paper Th4A.16.

[8] F. Roth, C. Lupulescu, E. Darlatt, A. Gottwald, and W. Eberhardt, "Angle resolved Photoemission from Cu single crystals; Known Facts and a few Surprises about the Photoemission Process," J. Electron Spectrosc. **208**, 2-10 (2016).

[9] B. Dold and R. Mecke, "Optische Eigenschaften von Edelmetallen, Übergangsmetallen und deren Legierungen im Infrarot (1. Teil)," Optik**22,** 435–446 (1965).

[10] P. Winsemius, H. P. Langkeek, and F. F. van Kampen, "Structure dependence of the optical properties of Cu, Ag and Au," Physica**79B**, 529–546 (1975).

[11] G. Leveque, C. G. Olson, and D. W. Lynch, "Reflectance spectra and dielectric functions of Ag in the region of interband transitions," Phys. Rev. B **27,** 4654–4660 (1983).

[12] M. L. Thèye, "Investigation of the optical properties of Au by means of thin semitransparent films," Phys. Rev. B **2**, 3060-3078 (1970).

[13] Aleksandar D. Rakić, Aleksandra B. Djurišić, Jovan M. Elazar, and Marian L. Majewski, "Optical properties of metallic films for vertical-cavity optoelectronic devices," Applied Optics **37**, 5271-5284 (1998).

[14] C. Kittel, "Introduction to solid states," Wiley, New York, (1971).

[15] P. B. Johnson and R.W. Christy, "Optical constants of the nobles metals," Phys. Rev. B**6**, 4370-4379 (1972).

[16] A.Vial and T. Laroche, "Description of dispersion proprieties of metals by means of the critical points model and application to the study of resonant structures using the FDTD method,"

J. Phys. D. Appl. Phys. **40**, 7152-7158
(2007).

[17] A. Vial and T. Laroche,
"Comparison of gold and silver
dispersion laws suitable for FDTD
simulations," Appl. Phys. B **93**, 139-149
(2008).

[18] J.Y. Lu and Y.H. Chang,
"Implementation of an efficient
dielectric function into the finite
difference time domain method for
simulating the coupling localized
surface plasmons of nanostructures,"
Superlattices and Microstructures **47**,
60-65 (2009).